

MEASUREMENTS OF RESIDUAL STRESSES IN COLD-ROLLED 304 STAINLESS STEEL PLATES USING X-RAY DIFFRACTION WITH RIETVELD REFINEMENT METHOD

Parikin^{1*}, P. Killen² and A. Raftery²

¹Center For Technology of Nuclear Industry Material
National Nuclear Energy Agency (BATAN), Serpong

²Department of Physics, Queensland University of Technology, Brisbane Australia

Received 14 March 2008; Received in revised form 13 October 2008; Accepted 6 November 2008

ABSTRACT

MEASUREMENTS OF RESIDUAL STRESSES IN COLD-ROLLED 304 STAINLESS STEEL PLATES USING X-RAY DIFFRACTION WITH RIETVELD REFINEMENT METHOD. The determination of the residual stresses using X-ray powder diffraction in a series of cold-rolled 304 stainless steel plates, deforming 0, 34, 84, 152, 158, 175 and 196 % reduction in thickness has been carried out. The diffraction data were analyzed using the Rietveld structure refinement method. The analysis shows that for all specimens, the martensite particles are closely in compression and the austenite matrix is in tension. Both the martensite and austenite, for a sample reducing 34% in thickness (containing of about 1% martensite phase) the average lattice strains are anisotropic and decrease approximately exponential with an increase in the corresponding percent reduction (essentially phase content). It is shown that this feature can be qualitatively understood by taking into consideration the thermal expansion mismatch between the martensite and austenite grains. Also, for all cold-rolled stainless steel specimens, the diffraction peaks are broader than the unrolled one (instrumental resolution), indicating that the strains in these specimens are inhomogeneous. From an analysis of the refined peak shape parameters, the average root-mean square strain, which describes the distribution of the inhomogeneous strain field, was predicted. The average residual stresses in cold-rolled 304 stainless steel plates showed a combination effect of hydrostatic stresses of the martensite particles and the austenite matrix.

Keywords: 304 stainless steel, cold rolling, X-ray diffraction, Rietveld refinement method, and residual stress.

© 2009 Atom Indonesia. All rights reserved.

INTRODUCTION

In recent industrial developments, cold rolling fabrication of metals has an important role that cannot be separated from the chain productions. The requirements of different shape and thickness in the building construction lead to give the convenience of easy installation of utility service. However, the presence of such fabrication may change the stress distribution within the materials, especially near surface regions. These internal stresses are called residual stresses and defined as the stresses that

* Corresponding author.
E-mail addresses: farihin@batan.go.id (Parikin)

would still exist in elastic solid body if all external loads (i.e. cold forming) were removed [1].

Cold forming process of 304 stainless steels can lead martensitic transformation, $\gamma \rightarrow \alpha$, which can cause a significant change in the mechanical properties of the material. The proportion of transformed $\gamma \rightarrow \alpha$ can be observed by means of Rietveld method, where phases (austenite-martensite) in the specimens are analyzed. The induced strains can also be evaluated from the lattice and full width half maximum (FWHM) parameters using shearer's line broadening analysis [2]. This analysis can give quantities of residual stresses.

The residual stresses are the elastic forces that change the interplanar spacing of crystal planes without applied external load. The small change can only be observed by using diffraction techniques. X-rays, having the same order in wavelength with the interplanar spacing, can measure the changes. As the X-rays have no charges, they may penetrate into materials in certain distance. By providing the diffractometer and Rietveld analysis, observation of the phases for measuring the residual stresses in the materials can be successfully performed. The methods are one of the most reliable technique that can be applied to determine the residual stresses in the steel plates. This may lead to the way in the quality control process and the investigation of end-products.

In the Rietveld method the least square refinements are carried out until the best fit is obtained between the entire observed (powder) diffraction pattern taken as a whole and the entire calculated pattern based on the simultaneously refined models, diffraction optic effects, instrumental factors, and other specimen characteristics (e.g. lattice parameters) as may be desired and can be modelled. A key feature is the feedback, during refinement, between improving knowledge of structure and improving allocation of observed intensity to partially overlapping individual Bragg reflections.

The presence of residual stresses can be beneficial or detrimental to strength of a component depending upon their sign and magnitude and the type of loading experienced by component. A residual stress distribution that augments the applied stresses, will be detrimental, and one which opposes, by acting in the reverse direction to the applied stresses, will be beneficial. For cyclic loading, in tension, tensile surface residual stresses can be particularly harmful since they may aid crack initiation and growth when subjected to fatigue stresses. Manufacturing processes that leave compressive stresses, crack inhibiting and residual surface stresses are therefore often chosen for components experiencing this type of loading. For instance, thick-walled plates, there are, to be subjected oftenly by external load are frequently auto-frettaged prior to use to develop compressive residual stresses at a construction to enhance fatigue life. Because of the influence of the residual stresses on component behaviour and the purpose of applying both

diffraction technique and Rietveld analysis in determining microstrains, it is desirable to know their distributions and its averaged magnitudes.

This paper describes the residual stress measurements of cold-rolled 304 steel plates by using X-ray diffraction and Rietveld refinement method. The crystallographic data were evaluated and matched between observation (experiments) and calculation (Rietveld program) and then predicted the stresses in the materials by formula appropriately. The presented study is aimed to obtain safe materials for its application as high temperature component of nuclear power plant turbine.

THEORY

Diffraction methods measure components of strain directly from changes of the lattice spacing of crystals. The residual stresses are then calculated from these strains. X-ray diffraction method is a powerful non-destructive techniques for characterizing residual stresses in crystalline materials [3]. When a material is subjected to a homogeneous strain field, the angular position of a peak will shift to lower or higher 2θ values, depending on whether the strain is tensile or compressive. If the material is subjected to an inhomogeneous strain field, then in addition to a possible shift in the peak position, the diffraction peak profile will also be broadened. Thus, while the shift of a peak measure the average lattice strain along particular crystallographic direction, the breadth of the peak provides useful information about the distribution of fluctuation of the inhomogeneous strain field. From the experimentally determined strains, the residual stresses can be deduced using appropriate models.

The penetrating capacity of X-ray is particularly important in studies of the residual stresses in the near surface region. It is well recognized that high angular resolution is desirable for precise strain measurements. By using the Rietveld analysis, the precision of the strain measurements can be further improved. In a Rietveld analysis, the entire observed diffraction pattern is fitted with a pattern calculated from an assumed structure model. Since a large number of diffraction peaks are fitted simultaneously, the statistical errors introduced in individual peak fitting are largely reduced. Moreover, by fitting to the whole pattern, any effects of preferred orientation, extinction, and other systematic aberrations, will also be minimized [4]. The average lattice strain along a particular crystallographic direction, $[hkl]$, is given by:

$$\varepsilon_{hkl} = \frac{d - d_0}{d_0} \quad (1)$$

where d and d_0 are, respectively, the lattice spacing of the stressed and stress-free (reference) samples along $[hkl]$. In the present experiment, the volume averaged lattice strains along various $[hkl]$ conform to the crystal

symmetry, as would be expected for strains arising solely from the mismatch of the random orientation of the grains in the specimens. In general, a strain tensor has six independent components, but when the strain tensor conforms to crystal symmetry, the number of independent component will be reduced. For uniaxial crystal structures, as in the case for both austenite and martensite, only two independent components are needed to represent the strain tensor properties completely [5]. Strains along any other directions can be calculated using tensor algebra. It is chosen to determine the strain components along the principal axes which are the a and c axes in the conventional structure setting for austenite and martensite.

The strains discussed above are the average values over the entire irradiated volume. The residual stresses in most solid aggregates are, however, far from homogeneous. As mentioned earlier, the presence of inhomogeneous strain field results in broadening of the diffraction profile. In general, peak broadening can be ascribed to either a small particle size or an inhomogeneous strain field, or both. Typically the broadening due to small particle size appears in the form of a Lorentzian whereas that due to inhomogeneous strain field is described by a Gaussian function.

The broadening of a diffraction peak due to the presence of an inhomogeneous [6] strain field is given by:

$$\begin{aligned} B^2 &= B_0^2 + 32 \ln 2 e_{av}^2 \tan^2 \theta \\ &= U \tan^2 \theta + V \tan \theta + W \end{aligned} \quad (2)$$

where B is the FWHM of the broadened peak and B_0 is the instrument resolution which varies with θ according to the Cagliotti [7] equation,

$$B_0^2 = U_0 \tan^2 \theta + V_0 \tan \theta + W_0 \quad (3)$$

Since only a modest R factor was achieved in the refinement, it is impractical to model the anisotropic inhomogeneous strain field with the present experimental data. Here, a simpler approach is taken to obtain an estimate of \bar{e} , the average value of the anisotropic *rms* strains within the specimens. Substituting Eq.(3) into Eq.(2), it can be obtained,

$$U = U_0 + 32 \ln 2 e_{hkl}^2 \quad (4)$$

Equation (4) indicates that \bar{e} can be estimated from the refined peak shape parameter U , where e_{hkl} is value of the anisotropic strains within any directions In the calculations, the parameter U_0 was taken from the refinement of the unrolled specimen standard. Here, U, V, W, U_0, V_0 and W_0 are constants of the equations.

Now that the lattice strains have been characterized, the residual stress in each phase can be deduced. Since no pressure was applied during the experiment, the residual stresses in each phase are expected to be hydrostatic. In fact, for obtaining the average lattice strains discussed above, from the refinement of a diffraction pattern over a wide angular range and hence represented some kind of average over many directions in the diffraction plane, it is better to measure the hydrostatic stress rather than the stress along particular specimen orientation. The hydrostatic stress, σ , is related to the hydrostatic [8] strains, $\bar{\epsilon}$, by the following equation:

$$\sigma = \frac{E}{1-2\nu} \bar{\epsilon} \quad (5)$$

where E is Young's modulus and ν is Poisson's ratio of the specific material considered. The given parameters[9] for the 304 stainless steel are 187 GPa and 0.293 respectively. For a hydrostatic stress state, $\bar{\epsilon}$ can be calculated along any direction with respect to the specimen orientation, $\bar{\epsilon} = (1/4\pi) \int_{\Omega} \epsilon_{hkl} d\Omega$, where ϵ_{hkl} is the strain within the grain whose $[hkl]$ lies in the direction under consideration and the integration is performed over randomly oriented grains. It is shown that for martensite phase, that equation becomes,

$$\bar{\epsilon} = \frac{1}{3} [2\epsilon_a + \epsilon_c] \quad (6)$$

where ϵ_a and ϵ_c are the strain in the direction of a -axis and c -axis respectively. In the calculation for the strain of austenite phase, the second order becomes ϵ_a and the average value is, hence, similar to the lattice strain itself.

The residual stresses in martensite particles and austenite matrix are not independent. Rather, they are governed by the equation of equilibrium [8],

$$f_a \sigma_a + f_m \sigma_m = 0 \quad (7)$$

where f_a and f_m are the volume fractions of austenite and martensite phases respectively. Equation (7) can be used to check whether the hydrostatic assumption is valid.

EXPERIMENT

Materials Preparation

The type of AISI 304 (ASTM) standard sample is chosen to perform the experiments. The study consisted of experimental and analytical investigations of the structural of the 304 stainless steel plates, which have been rolled in room temperature with a reduction rate of 0.1 mm from about 1.25 cm to about 0.05 cm and about 1.01 cm. These correlate to the percentage of reduction about 0% (R000), 34% (R034), 84% (R084), 152% (R152), 158% (R158), 175% (R175) and 196% (R196). The percentages of reduction are calculated by formula: $\epsilon(\%) = 100\% \ln (T_0/T)$, where T_0 is the initial thickness and T is the thickness after rolled. This specification is well introduced in the optimum design of structures of sheets and railroad side ports, where higher physical properties are requested.

Equipments and Method

The rolled and unrolled (R000) specimens were scanned by X-ray diffractometer XD610-Shimadzu at PTBIN-BATAN to obtain the patterns. To minimise anisotropic scattering due to the presence of texture, the specimens were placed on the rotator (200-300 rpm). The obtained diffraction scans were analysed by the Rietveld method, obtaining the lattice and the U parameters. The average strains can be calculated from these parameters and then average stresses [10] as well. The structure data analysis was performed using the General Structure Analysis System (GSAS), a Rietveld structure refinement program developed by Allen C. Larson and Robert von Dreele [11], which is capable to handle powder diffraction data obtained by X-ray or Neutron spectroscopy [12].

RESULTS AND DISCUSSION

Rietveld Refinement

In Figure 1, the patterns of raw scanning X-ray diffraction data with insets the refinement for R000 (unrolled), R158, and R196 specimens are shown to simplify presenting study. In the insets, there are two marks of line broadening. The line below both patterns (raw and model) is indication of martensite phase positions, whereas the line above residual pattern is position of austenite phase.

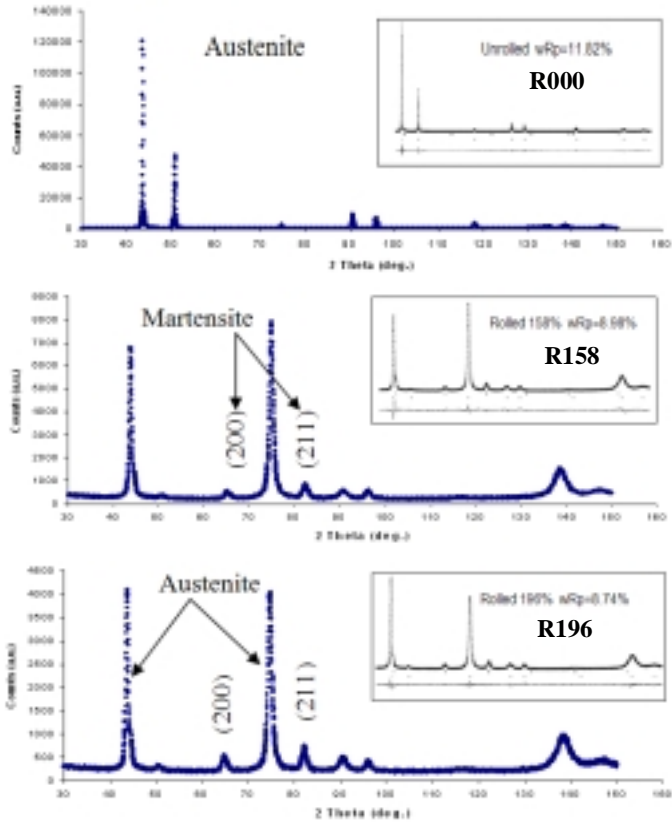


Figure 1. The raw scanning X-ray and the inset refinement patterns of R000 (unrolled), R158, and R196 specimens. The (200) and (211) reflections, indicate the growth of martensite. wRp is the value of fitted profiles between observation and calculation.

It can clearly be seen from (200) and (211) reflections that the martensite phase grows as an increase in the percent reductions. Since there was no evidence of martensite phase in the X-ray diffraction patterns, the unrolled specimen was assumed to be fully face centered cubic. The refinement was undertaken using a two-phase model consisting of the austenite phase (γ -Fe) with the space group Fm3m (I-225) and the martensite phase (α -Fe) using the body centered tetragonal with the space group I4/mmm (I-139). Initial lattice parameters was predicted from carbon content in stainless steel, using relations $a = 3.555 + 0.044x$ for austenite structure, and for martensite structure $a = 2.867 - 0.013x$ and $c = 2.867 + 0.116x$, where x is weight percent of carbon [2]. Table 1 gives the initial refined crystal structure parameters for the phases in the specimens.

Table 1. Initial refined crystal structure parameters for specimens.

Crystallographic Data	Austenite	Martensite
Formula	γ -Fe	α -Fe
Space Group	Fm3m (I-255)	I4/mmm (I-139)
Lattice Parameter : $a(\text{\AA})$	3.55764	2.86622
$b(\text{\AA})$	3.55764	2.86622
$c(\text{\AA})$	3.55764	2.87396
Cell Volume (\AA^3)	45.0283	23.6102
Number of Formula, Z	4	2
Mass Number of Formula, M (amu)	55.8450	55.8450

The peak shape profile of each phase was modelled separately using a pseudo-Voigt function (a linear combination of Gaussian and Lorentzian functions). The angular coverage of the experimental data was adequate to allow the structural parameters for each phase to be refined. These include lattice parameters, isotropic thermal parameters, zero point shifts, anisotropic (preferred orientation) parameters and profile parameters. The refinement of this two-phase model was satisfactory for each sputtered specimen, with the wRp ranging from 7% to 11% (listed in Table 2). The refined lattice and profile parameters for both the austenite and martensite phases vary little from specimen to specimen. In addition, reasonable thermal parameters were also obtained from the refinement, which have positive value. A complete set of refined structural parameters was read from database in the GSAS software. Insets in Figure 1 show the refined structural patterns with the residual appearances that indicate the fitted profiles (model) with the experimental data for three of the specimens.

Average Lattice Strains

A summary of refined lattice parameters and volume fraction of the phases is given in Table 2. Meanwhile Figure 2 illustrates the martensite growth, predicted by Rietveld refinement analysis. The martensite volume fraction can be calculated from scale factor of each phase, using relation; $W_m = (SZV)_m / \{(SZV)_a + (SZV)_m\}$ [4,13-14] where S, Z, and V are the scale factor, number of formula per unit cell and unit cell volume, respectively. Whereas subscribe m and a , indicate martensite and austenite phases. The fraction of martensite on surface shows an increase as addition in cold rolling. It is also compared by previous study of Llewellyn and Murray [15], which indicates small deviates with empirical prediction curve, showing by regression line.

Table 2. Refined room-temperature lattice parameters and volume fraction.

Specimens	Reduction (%)	$\hat{w}Rp$ (%)	Volume Fraction (%)		Lattice Parameters (Å)		
			Austenite	Martensite e	Austenite a(Å)	Martensite a(Å)	Martensite c(Å)
R000	0	11.82	100	0	3.59408	2.865401	2.905771
R034	34	9.25	99.07	0.93	3.597592	2.866532	2.905792
R084	84	9.31	93.62	6.38	3.596142	2.866868	2.905961
R152	152	9.41	77.38	22.62	3.595874	2.865810	2.905958
R158	158	8.98	75.46	24.54	3.595945	2.865632	2.905886
R175	175	7.67	69.58	30.42	3.596228	2.865056	2.905558
R196	196	8.74	61.45	38.55	3.596748	2.864194	2.904827

$\hat{w}Rp$ is the value of fitted profiles between observation and calculation.

In fact that lattice parameter has correlation with the interplanar spacing, equation (1) is similarly used to calculate the average lattice strain along particular crystallographic directions, where d and d_o are replaced by a and a_o or c and c_o respectively. The lattice a and c are the lattice spacing of the stress and the lattice a_o and c_o are the lattice spacing of the stress-free (reference) along $[hkl]$.

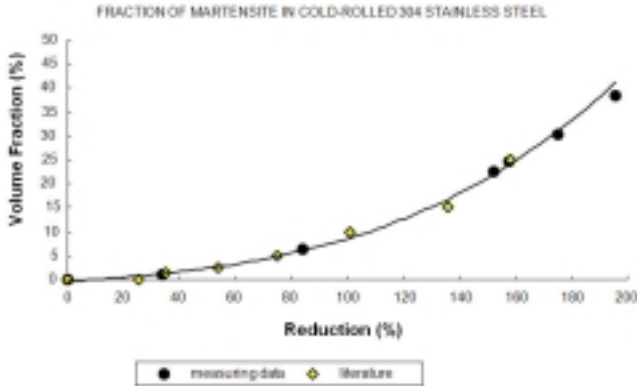


Figure 2. Martensite volume fraction as addition in percentage of reduction.

In the present experiment, good fits ($wRp= 7-11$ %) to the diffraction data were obtained for each stainless steel specimen. This result implies that, to within the experimental precision, the volume averaged lattice strains along various $[hkl]$ conform to the crystal symmetry, as would be expected for strains arising solely from the mismatch of thermal expansion in a mixture of randomly oriented grains. In this case the strain tensor conforms to the crystal symmetry, the number of independent components will be reduced into one and two independent component. In the uniaxial crystal structures, as in austenite structure, only one independent component is needed and in martensite structure only two independent components are required to represent the strain tensor properties completely [5]. Along any

other directions, strains can be computed using tensor algebra. It is desirable to determine the strain components along the principal axes which are a axis for austenite phase and a and c axes for martensite phase in the conventional structure setting. The results are listed in Table 3.

Table 3. Average lattice strains along major crystallographic directions.

Specimens	Average Lattice Strains (%)		
	Austenite	Martensite	
	$a//$	$a//$	$c//$
R000	0	0	0
R034	0.097713	0.039467	0.000736
R084	0.057364	0.051197	0.006535
R152	0.049919	0.014257	0.006450
R158	0.051887	0.008070	0.003961
R175	0.059773	-0.012030	-0.007320
R196	0.074232	-0.042130	-0.032480

It can be seen in Table 3 that austenite matrix was in tension, while both a and c in martensite particles (in column 3 and 4) show closely in similar compressive tendencies i.e. the values of strain became negative in R175 and R196. Furthermore, the measured strains in each phase are strongly anisotropic. For martensite particles, $|\epsilon_c| < |\epsilon_a|$ and in contrast the austenite (matrix) lattice strains experienced much tension as compared to the martensite (particle) lattice strains. These features can be qualitatively understood by considering the thermal expansion mismatch between the austenite matrix and the martensite particles in which the heat is generated as cold rolling is conducted. Since the strain measured in a diffraction experiment is an averaged value over a macroscopic sampling volume, an appropriate average of matrix and particle thermal expansion needs to be taken in order to model the experimental data. The evaluation of the lattice strains in the austenite matrix and martensite particles, then, can be done by interchanging of thermal expansion. Table 4 gives the values of thermal expansion coefficients, α , for stainless steels [16].

Table 4. Thermal expansion coefficients used for estimating the anisotropic lattice strains

Type	Thermal expansion coefficient, α ($\times 10^{-6}$ / $^{\circ}$ K)	
	High	Low
Austenitic stainless steel	18	16
Martensitic stainless steel	12	10
Stainless steels (bulk)	19	11

According to Eshelby's inclusion theory [17], the elastic strain, inside uniformly dispersed particles, can be written as $\epsilon \approx C(\alpha_m - \alpha_p)(T_E - T_{room})$. C is a constant with a complex function of many variables that can firstly be

neglected in the discussion of anisotropic (particle-matrix) thermal expansion and T_E (1050°C) is an effective freezing temperature below which no stress relaxation occurs. In the cold-rolled 304 stainless steel plates containing a small fraction of martensite particles, each martensite grain on average can be regarded as surrounded by randomly oriented austenite grains. In this case the matrix thermal expansion coefficient should be replaced by the bulk averaged thermal expansion coefficient. With this assumption it can be indicated that the average lattice strains in the austenite matrix are in tension, since the thermal expansion coefficient is larger than the martensite particle thermal coefficient. The prediction is consistent with the experimental data shown in Figure 3.

The calculated ratio of ϵ_c/ϵ_a (in Tabel 3) for martensite phase increases, dependent of the martensite volume fraction (in Tabel 2). As a result of cold rolling the martensite volume fraction rises, an increasing difference is observed as the experimental ϵ_c/ϵ_a becomes increasingly larger. A possible cause for the observed difference is that as the martensite particles become increasingly interconnected with each other so that the particles thermal expansion parameters used in the relation need to be modified to take this effect into consideration. The thermal expansion martensite particle should be replaced by the bulk averaged thermal expansion coefficient. Furthermore, another survived argumentation that is, the larger range of bulk thermal expansion is reasonable interpretation in the compressive residual stresses why they little shift glimpse from the negative values. The bulk thermal expansion ranges from $19 \times 10^{-6} / ^\circ\text{K}$ to $11 \times 10^{-6} / ^\circ\text{K}$. It is supposed that the lower value dominates when the reduction in thickness below about 160%, while the higher value will effectively influence at above the percentage. This leads to negative strain in the martensite particles as addition in cold rolling. These are consistent with the experimental observation for martensite phase. The small values of the measured lattice strains, however, preclude us from comparing either ϵ_c/ϵ_a or ϵ_a/ϵ_c because the estimated standard deviations of these ratios are too large. Clearly, for a quantitative analysis of anisotropic strain data, an explicit expression for the coefficient C is required.

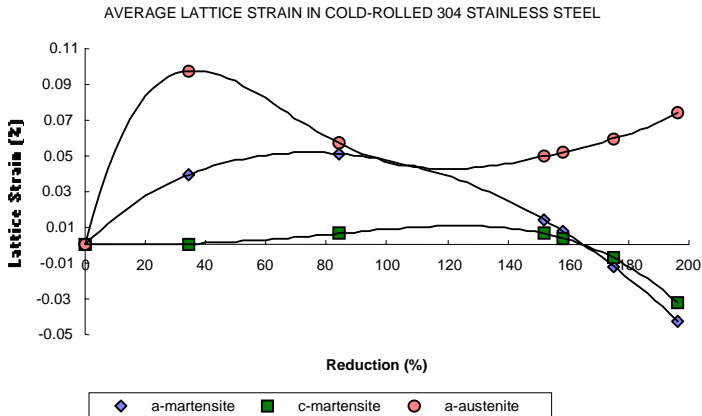


Figure 3. Experimentally determined average lattice strains as a function of percent reduction (essentially volume fraction of martensite phase).

In addition, the degree of connectivity of the martensite particles will also need to be carefully examined. As seen from Table 2 and Table 3, for each martensite volume fraction that the average lattice strains may not vary, to within the experimental precision, with the martensite grain size over the range covered in the present experiment. This result is, in fact, consistent with micromechanic analyses, which suggest that the lattice strains are not significantly altered by small changes in grain sizes. Since the lattice strains are insensitive to changes in grain sizes. As indicated in Figure 3 the specimen-averaged lattice strains in both phases vary in a polynomial fashion with the percentage of reduction and essentially the martensite volume fraction. This behaviour is in agreement with predictions by the inclusion theory for metal containing a small fraction of inclusions, composite likelihood [17].

Peak Broadening and the *rms* Strains

The average strain values over the entire irradiated volume have been discussed above. In fact, the residual stresses in most solid aggregates are, however, far from homogeneous. As mentioned earlier, the present of an inhomogeneous strain field results in broadening in the diffraction profile. All stainless steel specimens studied in this experiment exhibit some degree of peak broadening. The values of strain fields are listed in Table 5, were calculated from equation (4) by using Gaussian model in the refinement method and plotted in Figure 4. The strain fields vary with the percent reduction of the specimens. The actual value of the strain fields is not negative. In the regression line of martensite strain field, it can be seen that

the line is through the negative value. This was suggested that martensite phase has not been formed below about 30% of reduction in thickness. Meanwhile, it shows that around 50% reduction, the strain field line of both phases slices each other, informing that at the intersection the strains could be regarded as a homogeneous condition (isotropic).

Table 5. Average *rms* strain ($\bar{\epsilon}$) deduced from the profile shape parameter U.

Specimen	Strain Fields, $\bar{\epsilon}$ (%)	
	Austenite	Martensite
R000	0	0
R034	0.069334	0.013721
R084	0.047824	0.138698
R152	0.06779	0.18769
R158	0.070692	0.196077
R175	0.07895	0.225168
R196	0.088784	0.271578

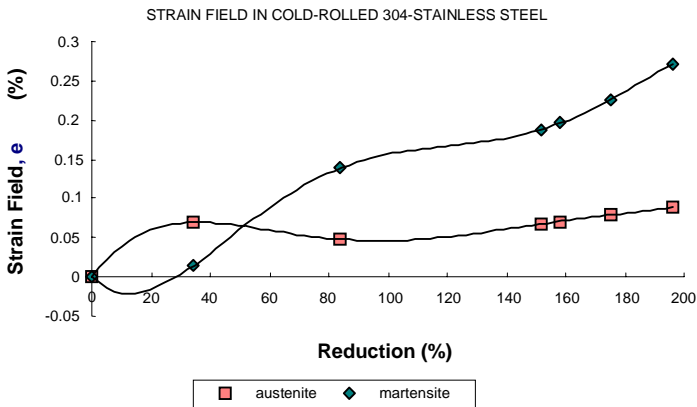


Figure 4. Strain fields as a function of the percentage of reduction in both phases of specimens.

Because of the limited range of the grain sizes, it is not anticipated that strain field, $\bar{\epsilon}$ varies with the grain size of either the austenite and martensite grains. It can be seen that for the austenite matrix, $\bar{\epsilon}$ closely follows the average lattice strains, ϵ_a . Meanwhile for martensite particles, in particular, $\bar{\epsilon}$ increases nearly linear with the increase of ϵ_c/ϵ_a and martensite volume fraction. This observation suggests that the inhomogeneous strain field in the austenite matrix result primarily from the inclusion of the martensite

particles. Further investigation, the anisotropic strain broadening was attributed to the concentration of dislocations associated with the close packed planes [18].

Moreover, the broadening appears to be particularly pronounced for the austenite peak. For the purpose of illustration, the (220) reflection from the R000 and R196 specimens is shown in Figure 5. A Gaussian fit to this peak is excellent. The fitted FWHM (full width at half maximum) is $0.843^\circ \pm 0.003^\circ$ significantly larger than unrolled specimen (the instrumental resolution) which is $0.342^\circ \pm 0.005^\circ$ in the 2θ range shown in the figure.

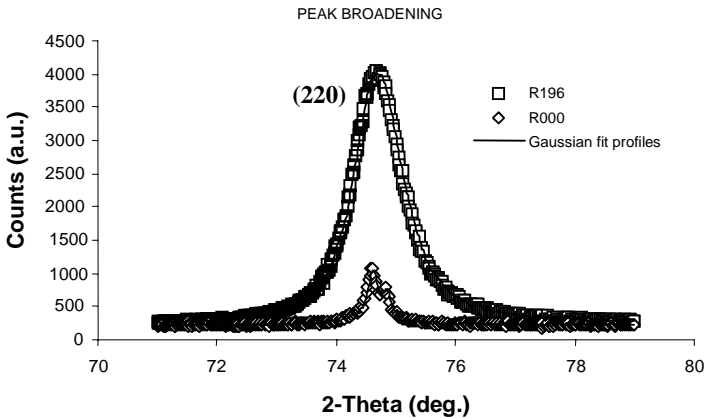


Figure 5. The (220) austenite reflection from specimen R000 and R196. The open squares and rectangles are experimental data and the solid curve is a Gaussian fit to the data. The instrumental resolution is clearly shown.

In general, peak broadening can be ascribed to either a small particle size or an inhomogeneous strain field, or both. Typically, the broadening due to a small particle size appears in the form of a Lorentzian whereas that due to the strain is described by a Gaussian function. The insets in Figure 1 have already demonstrated that the diffraction peaks can be well modelled with a Gaussian. Furthermore, the Rietveld analysis of the measured diffraction patterns revealed only a small fraction of Lorentzian component in the peak shape profile. It thus becomes clear that the observed broadening in cold-rolled 304 stainless steel specimens is largely due to an inhomogeneous strain field rather than the particle size. Also, as it can be observed from the profile of one-another, the diffraction peaks show a difference in curve widths. This suggests that the peak broadening is anisotropic. The origin of anisotropic strain broadening varies. For instance, the presence of defects along a particular $[hkl]$ gives rise to a spatial fluctuation of d_{hkl} within a grain,

leading to the broadening of reflection (hkl). The variation of d_{hkl} from grain to grain also contributes to the broadening of (hkl) planes.

Residual Stresses

The residual stresses in each phase can be deduced from the lattice strains that have been characterized. During the experiment, there was no pressure applied, the residual stresses in each phase are assumed to be hydrostatic. The average lattice strains, as discussed above, were obtained from the refinement of a diffraction pattern over a wide angular range. Hence, they represented some kind of average over many directions in the diffraction plane, are a better measure of the hydrostatic stress rather than the stress along a particular specimen orientation. The hydrostatic stresses, σ are calculated using equation (5). In this condition $\bar{\varepsilon}$, can be estimated along any direction with respect to the specimen orientation and was calculated using equation (6). The parameter E and ν used in the evaluation of σ were obtained from independent mechanical measurements in literature [9]. For type 304 stainless steel at room temperature, the extrapolated parameters are 187 GPa and 0.293, respectively. Figure 6 shows the hydrostatic stresses thus computed as a function of the percent reduction.

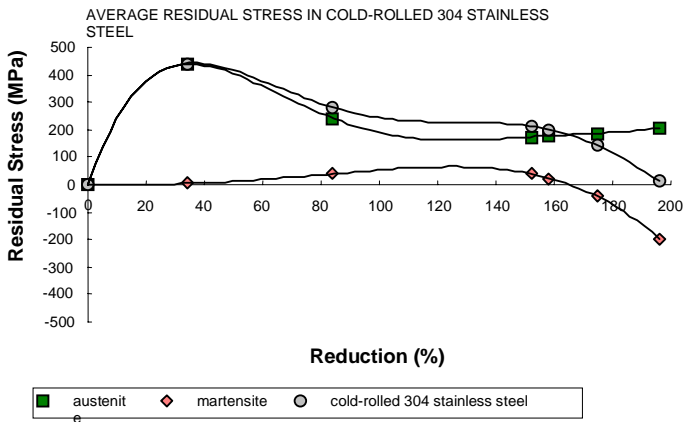


Figure 6. Hydrostatic stresses in cold-rolled 304 stainless steel plates as a function of percent reductions.

As expected from the behaviour of the lattice strains, the calculated hydrostatic stress in the martensite particles is closely in compression, although below around 160 % of reductions show a little in tension, while in the austenite matrix the stress is much in tension. In the specimen containing about 1.0 % martensite phase (cold-rolled 34%), the tensile stress is as high

as about 437.25 MPa in austenite matrix and about 4.43 MPa in martensite particles, and completely in that specimen the residual stress is about 442 MPa. For austenite matrix, the calculated hydrostatic stress tends to decrease whereas in martensite particle increases progressively in compressive hydrostatic stress with an increase in the percent reduction. However, the residual stresses in 304 stainless steel plates show a decrease as addition in thickness reductions. The line shows that below 100% reduction in thickness the plate residual stresses dominated by the matrix residual stresses, whereas above this reduction the particles residual stresses have more effects in plates. It can be interpreted that the more martensite formation occurs at the more cold reduction in thickness. These are well confirmed with the fact that the residual stress in the martensite particles and austenite matrix are not independent, rather than they are governed by the relation of equilibrium [8].

From the curve behaviour, it is reasonable that the hydrostatic stresses in the specimens at below 160 %reduction is dominated by stresses in the austenite matrix. Instead of above that percentage the martensite particles reveal its domination. This is a very well conformation with the information of the strain field shown in Figure 4, that the martensite strain field gradually increases while the austenite strain field slowly rises and even tends to be flat. This stress characteristic is also observed in several specimens of Assab Corrax steel and discussed in recent laboratory report of the steel, which exhibits equilibrium stresses [19,20].

CONCLUSIONS

In summary, demonstration of X-ray powder diffraction technique coupled with the Rietveld analysis provides a powerful experimental method for the determination of the residual stresses in stainless steel specimens. The method is applied to study of a series of cold-rolled 304 stainless steel plates. A good fits (wRp : 7-11%) was obtained, made the predictions much reliable. From an analysis of anisotropy of measured lattice strains, it was established that the residual stresses in these specimens were primarily due to thermal expansion mismatch between martensite and austenite. As a result of this mismatch, the martensite particles are closely in compression and the austenite matrix is in tension. The average lattice strains in each phase vary approximately by a part of quadratic and exponential with an increase in the percent reduction (essentially volume fraction of martensite phase). This was in agreement with the predictions by the inclusion theory. From the experimental strain data, the residual stresses in both phases were evaluated. It was found the tensile residual stress in a specimen was quite large, reaching 442 MPa, for a sample reducing 34% in thickness (containing about 1% martensite phase). Whereas the improvement in martensite volume fraction, caused by reduction at room temperature, decreased the residual

stresses to following the residual stress patterns contained in martensite particles. For all stainless steel specimens, the diffraction peaks are broader than the unrolled specimen (instrumental resolution), indicating the presence of inhomogeneous strain field. Assuming a Gaussian distribution of the inhomogeneous strain field, the average value of the *rms* strains was determined from the refined peak shape parameters. The variations of the average *rms* strains with the martensite volume fraction suggest that the inhomogeneous strain field in the austenite matrix result primarily from the inclusion of the martensite particles.

There was a qualitative evidence from the measurements of residual stresses and subsequent analysis of the material that the cold-rolled 304 stainless steel plates will be safe to be applied as high temperature component of nuclear power plant turbine, as there was no significant residual stress effects observed in these materials after the rolling process.

ACKNOWLEDGMENTS

The writer would like to express his thanks to Ir. Iman Kuntoro, M.Sc., Dr. rer.nat Evy Kartini, Dr. Siti Amini, Pof .Drs. Sunarhadiyoso, M.Sc., Dr. Azis Khan Jahja, Drs Bambang Sugeng, M.T. and Mr. Imam Wahyono for their kindness and helpful.

REFERENCES

1. ALMEN, J.O. and P.H. BLACK, : "Residual Stresses and Fatigue in Metals", Mc Graw-Hill, New York, (1963).
2. CULLITY, B.D., : "Introductions to X-ray Diffraction", 3th ed. John Willey & Sons, New York, (1995).
3. CHRISTENSEN, A.L., (ed.), : "Measurement of Stress by X-ray", SAE Inform.Rept. TR-182 (1960).
4. HILL, R.J. and HOWARD, C.J., *J. Appl. Crystallogr.*, **20**, 467-74 (1987),
5. NYE, J.F., : "Physical Properties of Crystals", Oxford University Press, Oxford, UK, (1985).
6. KLUG, H.P. and ALEXANDER, L.E., : "X-ray Diffraction Procedures", 2nd ed., Willey, New York, 618-708 (1974).
7. CAGLIOTTI, G. ET AL., *Nuc. Instrum.*, **3**, 223-28 (1958).
8. NOYAN, I.C. and COHEN, J.B., : "Residual Stress Measurement by Diffraction and Interpretation", Springer-Verlaag, New York, (1987).

9. ANONYMOUS, : "Properties and Selection: Irons, Steels and High Performance Alloys", Metals Handbook, **1**, 10th ed., ASM International, New York, (1990).
10. PARLANE, A.J.A., : "The Determination of Residual Stresses: Residual Stresses in Welded Construction and Their Effect", Welding Institute, Cambridge, 63-78 (1978).
11. LARSON, A.C. and R.B.VON DREELE, : "General Structure Analysis System", LANSCE, MS-H805, Los Alamos National Laboratory, Los Alamos, NM 87545, University of California, (1994).
12. YOUNG, R.A., : "The Rietveld Method", IUCr Book Series 5, International Union of Crystallography, Oxford University Press., UK, (1997).
13. LUTTEROTTI, L. and P. SCARDI, *J. Appl. Crystallogr.*, **23**, 246-252 (1990).
14. PARIKIN ET.AL., Study of α' -Martensite Growth in Hardened 304 Stainless steel, unpublished paper, (1997).
15. LLEWELLYN, D.T. and J.D. MURRAY, ISI Special Report 86, 197,(1964), in Steels: Metallurgy & Applications, 2nd ed., Butterworth-Heinemann, UK, (1992).
16. ANONYMOUS, : "Welding, Brazing, and Soldering", ASM Handbook, 6, ASM Internasional, New York, 903 (1994).
17. MORI, T. and K. TANAKA, *Acta. Metall.*, **21**, 571-574 (1973).
18. HALMOS, G.T., : "High Production Roll Forming", SME, Michigan, (1983).
19. PARIKIN, M. DANI, A.H. ISMOYO, N. EFFENDI and A. K. JAHJA, *Jurnal Teknik Industri*, **6** (1) 1-14 (2005).
20. PARIKIN and A.H. ISMOYO, *Jurnal Konduktor Padat*, **6** (1), 61-70 (2005).